Progress In Electromagnetics Research B, Vol. 59, 269–289, 2014

Calculation of the Mutual Coupling Parameters and Their Effects in 1-D Planar Almost Periodic Structures

Bilel Hamdi[1, 2, *], Taoufik Aguili[1], Nathalie Raveu[2], and Henri Baudrand[2]

Abstract—This paper proposes a new modal analysis based on Floquet's theorem which is needful for the study of a 1-D periodic phased array antenna excited by arbitrary located sources. This analysis requires an accurate estimation for calculation of the mutual coupling parameters (for example: mutual impedances or admittances ...) between the array elements and their effects integrating a large planar radiating structure. Two different formulations are suggested, in spectral and spatial domains, to solve the problem and to calculate the coupling coefficients between the neighbouring elements in a periodic environment. Important gain in the running time and used memory is obtained using Floquet analysis. One numerical method is used for modeling the proposed structures: the moment method combined with Generalized Equivalent Circuit (MoM-GEC).

1. INTRODUCTION

Actually, the modeling of periodic and almost periodic planar structures has been extensively the subject of considerable research for a long time especially in communication systems as satellite and radar applications, wavelength and polarization selective components in microwave, millimeter-wave and optical wave regions [2–4, 7 11 28].

Furthermore, various numerical techniques have been proposed to study any given structure for solving partial differential equations with periodic boundary conditions. Examples are the finite element method (FEM), the method of moment (MoM) and finite differences in the time domain method (FDTD) [1, 3, 28].

Therefore, we are interested in the mutual coupling for estimating the performance of an array antenna. Several articles show that it is impossible to get rigorous result when dealing with the mutual coupling problems: element-by-element method and infinite periodic structure method [2, 16]. To take coupling effects into account, a new modal analysis is necessary [10].

This work proposes an efficient approach to deal with the 1-D periodic micro-strip lines excited by located sources, when the Floquet's theorem asserts that the impressed fields are periodic and that the radiated fields have discrete spectra in the wavenumber space. The field components can be therefore expressed in the generalized Fourier series expansions, and the analysis region can be reduced to only one periodicity cell.

The field sources arrangement verifies the periodicity of the problem. Thus, as all approaches for periodic structures do, the usual techniques based on direct application of Floquet's theorem are applicable. Then most of the approaches for periodic structures are based on the Floquet theorem.

This fact increases the complexity of the problem of the investigated problem and fitting the modal analysis of the periodic structure being excited [2, 13, 15, 16].

Received 11 February 2014, Accepted 4 April 2014, Scheduled 15 May 2014

* Corresponding author: Bilel Hamdi (hamdibilel1985@gmail.com).

[1] Laboratory of the Communication Systems, National Engineering School of Tunis, B. P. 37, Le Bélvedere, Tunis 1002, Tunisia.

[2] Laplace Laboratory, ENSEEIHT, 2 rue Camichel, Toulouse Cedex 4, 31071, France.

This study shows some fundamental properties of the impressed electromagnetic fields in arbitrary located sources for periodic structures and introduces the periodic Fourier transform to approach the scattering problem of periodic structures in the spectral-domain [8, 11, 14].

For many structures, the method of moments (MoM) represents a suitable technique for computing the coupling between elements.

Our main goal here is to compute the current density lying on the strip lines considering the periodic boundary conditions and to deduce the mutual coupling parameters between array elements.

Due to the adoption of the modal analysis based on the Floquet states, the spectral formulation using the MoM-GEC results in a very important gain in the running time and used memory.

This paper is organized as follows. In Section 2, the background including the theoretical Floquet modal analysis is reviewed. First, the Finite Fourier Transform (FFT) and the spectral decomposition of the located source and the relevant 1-D and 2-D structures are given. The studied structures and the problem formulation are recalled in Section 3. It explains the manner that extracts the equivalent circuit which contributes to obtaining the integral equation based on the impedance operator using Generalized Equivalent Circuit (GEC). The following section illustrates the numerical results and discussions for the convergence of the Floquet impedance, input impedance viewed by located source, the convergence of current density on the strip line and the mutual coupling ($S_{i,j}$) data between 1-D periodic elements which are computed using two different formulations (spectral and spatial formulations) and compared to Ansoft HFSS, where the scan blindness occurs. This modal procedure minimizes the computation time and memory consumption considerably compared to the classical spatial case.

2. THEORY AND BACKROUND

2.1. Setting of the Problem

The global structure (or reference structure) under consideration is schematically shown in Figure 1 and composed of finite (or infinite) periodic phased array planar strip-lines with their own excitations (arbitrary located voltage sources). All elements are shielded in waveguide composed of two perfect electric boundaries along y-direction and by convenient boundary conditions along the x-direction which can be chosen from the following options: (a) Perfect Electric boundaries, (b) Perfect Magnetic boundaries, (c) Periodic boundaries with null phases shift, and (d) a combination of these boundary conditions. The top and the bottom are respectively an open circuit and a ground plane. The considered planar circuit is lossless.

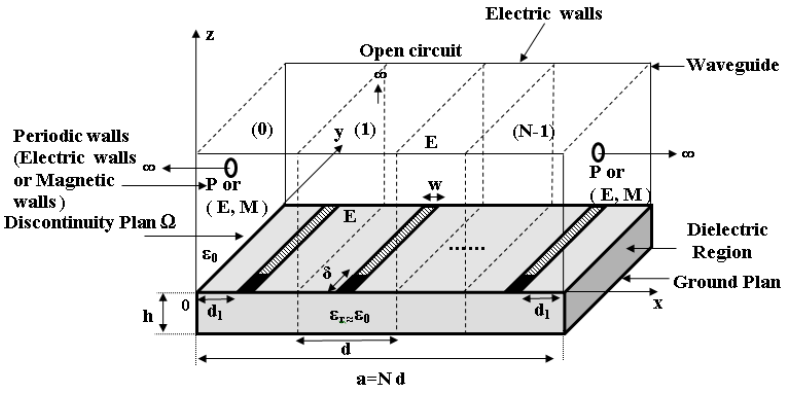

Figure 1. A section of periodic phased array micro-strips line.
EEEE: waveguide with electric walls
EMEM: waveguide with two electric walls and two magnetic walls
EPEP: waveguide with two electric walls and two periodic walls

Really, any radiator element placed next to another one, which is itself a radiator, allows to change the electromagnetic behavior and even deteriorate it.

For this configuration, the electromagnetic interaction between these periodic elements results in the modification of the current densities lying on each metallic part and generates a change of the radio-electronic characteristics (radiation, input impedance, directivity, etc.).

Using the modal analysis, the periodic symmetry of the structure allows us to concentrate on one cell of the array. It is the reason that we take only a basic structure formed by elementary planar structure locally excited by a rectangular voltage source, bounded in convenient boundary conditions (rectangular dielectric waveguide), similar to the global structure along y direction and two periodic boundaries along x-direction. Also, the top and bottom are an open circuit and a ground plane.

The interaction and mutual coupling between cells are taken into account through periodic boundary conditions at the borders of the unit cell (Floquet's theorem).

We should characterize this unit structure by proper states (or proper phases) which are controlled by the Floquet's modes which permit to reconstruct a final state or a spatial state of the whole structure (global structure) by applying superposition theorem.

These proper states of the basic structure (unit cell) contain information about the determination of the mutual coupling parameters established between distinct elements which belong to reference structure (global structure).

The determination of $[S]$ matrix is more complex by using classical spatial method (direct manner), but it is sufficient to predict it by a simple Fourier Transform based on Floquet's modes to identify all mutual coupling.

The periodic walls delimiting any N_x cells (one-dimensional case) of the array are placed at the following positions:

$$\begin{aligned} x(i) &= id \\ -\frac{N_x}{2} &\leq i \leq \frac{N_x}{2} - 1 \end{aligned} \tag{1}$$

Thus, the central cell (basic) can establish an interaction with other elements along x-direction (respectively in the two directions on the left and right in bi-dimensional case), following a leaky-waves which cause a change for the current appearing on the surface of each cell.

2.2. Modal Analysis and Fourier Transform's Principle of Feeding Sources: Floquet's Theorem

Firstly, we will consider only the one-dimensional case of the located excitation's modal decomposition in the spectral domain, and generalization in two dimensions is very easy.

Provided that a one-dimensional structure (1-D) along x-axis, with N identical cells. Each cell is excited by a located source and placed periodically according to the (ox) direction as described in Figure 1.

This structure is taken as infinite in $(\pm x)$ and periodic with a period d. $E(x)$ represents a field reacting with periodic surface. As mentioned before, it is useful to consider the geometric periodicity forcing the field to be periodic.

More generally:

$$E(x + N_x d) = C^{N_x} E(x) \tag{2}$$

$C = a$ complex constant.

For boundedness,

$$\mid C \mid \leq 1 \tag{3}$$

In general

$$C = e^{+j\alpha d} \tag{4}$$

where $k_x = \frac{2m\pi}{d} + \alpha$ is a wavenumber.

In our case, only the amplitude of these sources varies from an element to another.

The study is based on one periodic cell with $e^{j\alpha d}$ phases and $-\pi \leq \alpha \leq \pi$, that entrains a dependence in mode α.

Next, we propose $\tilde{f}_\alpha(x)$ as a periodic function or solution of propagation's equation (can be an electric field or a current density), and the result can be written as [23]:

$$\tilde{f}_\alpha(x) = e^{j\alpha x} \sum_m \tilde{f}_{m,\alpha}\, e^{j\frac{2m\pi}{d}x} \tag{5}$$

Consequently

$$\tilde{f}_\alpha(x+d) = e^{j\alpha(x+d)} \sum_m \tilde{f}_{m,\alpha}\, e^{j\frac{2m\pi}{d}(x+d)} = \tilde{f}_\alpha(x) \tag{6}$$

where m and α correspond respectively to (1-D) Floquet's mode and spectral domain mode.

For an infinite structure, where α belongs to Brillouin domain:

$$\alpha \in \left[-\frac{\pi}{d}, \frac{\pi}{d}\right] \tag{7}$$

with:

$$d\alpha = \frac{2\pi}{L} \tag{8}$$

and

$$L = N_x d \tag{9}$$

So, it is important to indicate:

$$\frac{1}{N_x} = \frac{d}{2\pi} d\alpha \tag{10}$$

According to the superposition theorem, we can always note:

$$f(x) = \frac{d}{2\pi} \int_{\frac{-\pi}{d}}^{\frac{\pi}{d}} \tilde{f}_\alpha(x)\, d\alpha \tag{11}$$

Based on Floquet's theorem, any planar periodic function can be expanded as an infinite superposition of Floquet harmonics.

In the following modal formulation, α is considered continuous, which allows to study an infinite case, but in a practical structure we use the word 'real finite array' to refer to a physical finite case. For this reason, one difference has been found, the discretization of modal state (Floquet modes), which becomes:

$$\alpha_p = \frac{2\pi p}{L_x} \tag{12}$$

with

$$-\frac{N_x}{2} \leq p \leq \frac{N_x}{2} - 1 \tag{13}$$

$$L_x = N_x d \tag{14}$$

Similarly, we express the superposition theorem:

$$f(x) = \sum_p \tilde{f}_{\alpha_p}(x) \tag{15}$$

The FFT can be applicable: let us consider E_i a group of sources in each cell, so it is clear to assume that $\tilde{E}_{\alpha_p}$ can be a group of spectral values for the central cell against the p states. Next, we can find:

$$E(id) = \frac{1}{\sqrt{N_x}} \sum_{p=-\frac{N_x}{2}}^{\frac{N_x}{2}-1} \tilde{E}_{\alpha_p} e^{j\alpha_p(id)} \tag{16}$$

In fact, the IFFT is given below:

$$\tilde{E}_{\alpha_p}(0) = \tilde{E}_{\alpha_p} = \frac{1}{\sqrt{N_x}} \sum_{i=-\frac{N_x}{2}}^{\frac{N_x}{2}-1} E(id) e^{-j\alpha_p(id)} \tag{17}$$

While knowing this spectral distribution, we can note entirely:

$$J(id) = \frac{1}{\sqrt{N_x}} \sum_{p=-\frac{N_x}{2}}^{\frac{N_x}{2}-1} \tilde{J}_{\alpha_p} e^{j\alpha_p(id)} \tag{18}$$

The IFFT is written identically:

$$\tilde{J}_{\alpha_p}(0) = \tilde{J}_{\alpha_p} = \frac{1}{\sqrt{N_x}} \sum_{i=-\frac{N_x}{2}}^{\frac{N_x}{2}-1} J(id) e^{-j\alpha_p(id)} \tag{19}$$

Assuming that the spectral current density on metallic domain is known, the Floquet-input impedance is rapidly obtained when the mutual coupling effects between elements are taken into account by using periodic walls in one unit cell. However, the modal analysis makes it possible to apply the Fourier Transform principle to periodic feeding sources problem.

Also, the Finite (Discrete) Fourier transform (FFT or DFT) can be expressed with matrix-vector notation:

$$[\tilde{E}_{\alpha_p}] = TF[E(id)] \tag{20}$$

Respectively:

$$[\tilde{J}_{\alpha_p}] = TF[J(id)] \tag{21}$$

where the Fourier matrix F has elements

$$TF = w^{ip} \tag{22}$$

where w is a complex nth root of unity:

$$w = e^{-j\frac{2\pi d}{L_x}} = e^{-j\frac{2\pi}{N_x}} \tag{23}$$

It turns out that F is nearly its own inverse. More precisely, F^H, the complex conjugate transpose of F, satisfies

$$TF^H TF = N_x I \tag{24}$$

so

$$TF^{-1} = \frac{1}{N_x} TF^H \tag{25}$$

This allows us to invert the Fourier transform:

$$[E(id)] = \frac{1}{N_x} TF^H \left[\tilde{E}_{\alpha_p}\right] \tag{26}$$

Respectively:

$$[J(id)] = \frac{1}{N_x} TF^H \left[\tilde{J}_{\alpha_p}\right] \tag{27}$$

The $\frac{1}{N_x}$ scaling factor in the inverse transform is sometimes replaced with $\frac{1}{\sqrt{N_x}}$ scaling factors in both transforms.

How is $Z = Z(i, j)$ matrix calculated?

Usually, we use the spatial domain to explain interaction between neighbouring elements, but now it is enough to use the FFT which facilitates this kind of problem by calculating spectral impedance for each mode, then we obtain the main result rapidly by a simple transformation (32). Thus, we can set the following relations: First, we consider this spectral representation:

$$\left[\tilde{E}_{\alpha_p}\right] = \left[\tilde{z}_{\alpha_p}\right] \left[\tilde{J}_{\alpha_p}\right] \tag{28}$$

Or the entire spatial expression can be obtained by:

$$[E_{id}] = [Z_{ij}] [J_{jd}] \tag{29}$$

which leads to:

$$TF^{-1}\left[\tilde{E}_{\alpha_p}\right] = [Z_{ij}]\, TF^{-1}\left[\tilde{J}_{\alpha_p}\right] \tag{30}$$

Then, we have:

$$\left[\tilde{E}_{\alpha_p}\right] = TF\,[Z_{ij}]\, TF^{-1}\left[\tilde{J}_{\alpha_p}\right] \tag{31}$$

Finally, (31) compared to (28) results in the following relation:

$$[Z_{i,j}] = TF^{-1}\left[\tilde{z}_{\alpha_p}\right] TF \tag{32}$$

where $\tilde{z}_{\alpha_p}$ is a diagonal operator for input impedance of each Floquet mode. Following a similar procedure, the mutual admittance and the scattering parameters between periodic elements in an array environment can be obtained as:

$$[Y_{i,j}] = TF^{-1}\left[\tilde{y}_{\alpha_p}\right] TF \tag{33}$$

$$[S_{i,j}] = TF^{-1}\left[\tilde{s}_{\alpha_p}\right] TF \tag{34}$$

Another way of calculating the coupling data is proposed when we can refer frequently to the following expression to compute the scattering parameters as:

$$[S_{i,j}] = \left[\frac{Z_{i,j}}{Z_c} - I\right]\left[\frac{Z_{i,j}}{Z_c} + I\right]^{-1} \tag{35}$$

where $[Z_{i,j}]$ is the mutual impedance between two different elements located at $x(i) = id$ and at $x(j) = jd$. Z_c designates the reference impedance which is often chosen as $50\,\Omega$, and I is an identity matrix.

After studying the one-dimensional case, it is rather simple to describe a bi-dimensional case especially for finite number of planar dipoles [3].

The structure described in [3] is a generalization of the preceding case with more complex periodicities. The addition of the second direction makes two modes (α_p, β_q) in the spectral space when each element is surrounded by suitable periodic walls along (ox) and (oy) directions in order to tackle all elements.

3. PROBLEM FORMULATION

In this section, it is important to clearly explain the theoretical development to solve planar structure in periodic environment.

That is why two formulations are proposed in this work: The first is called spectral formulation which is based on studying the unit cell described in Figure 2. The second is a spatial formulation associated to a global structure given in Figure 1.

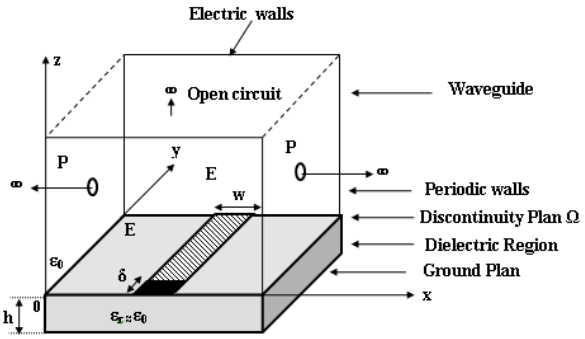

Figure 2. A unit cell of the whole structure.

3.1. Spectral Formulation

Whenever applied to periodic structures, the first step of this formulation is to study the elementary cell particulary, instead of treating the whole structure at once.

The environment of this studied structure is expressed by an impedance (or an admittance) operator corresponding to evanescent modes. It is important to note that the $\hat{Z}_\alpha$ expression following the Dirac notation is rewritten as:

$$\left[\hat{Z}^{upper,down}_{pq,st,\alpha}\right] = \left[\sum_{m,n} \langle g_{pq,\alpha}|f_{mn,\alpha}\rangle z^{upper,down}_{mn,\alpha} \langle f_{mn,\alpha}|g_{st,\alpha}\rangle\right] \tag{36}$$

and the inner product is given by:

$$\langle u|v\rangle = \iint_D uv^*\, ds \tag{37}$$

(* denotes the complex conjugate), and $|f_{mn,\alpha}\rangle$ represents the modes $|TE_{mn,\alpha}\rangle$ and $|TM_{mn,\alpha}\rangle$.

Here we will define a **new** expression of $|f^{TE,TM}_{mn,\alpha}\rangle$ functions, combined **electric-periodic** walls, which are:

$$\left\{\begin{array}{c} |TE_{mn,\alpha}\rangle \\ m \in Z \\ n \in N^* \end{array}\right\} = \left\{\begin{array}{l} \frac{k_{yn}}{\sqrt{k^2_{xm,\alpha}+k^2_{yn}}}\sqrt{\frac{2}{dL}} \\ \exp(+j(k_{xm,\alpha}x))\sin(k_{yn}y) \\ j\frac{k_{xm,\alpha}}{\sqrt{k^2_{xm,\alpha}+k^2_{yn}}}\sqrt{\frac{2}{dL}} \\ \exp(+j(k_{xm,\alpha}x))\cos(k_{yn}y) \end{array}\right. \tag{38}$$

$$\left\{\begin{array}{c} |TE_{m0,\alpha}\rangle \\ m \in Z^* \\ n = 0 \end{array}\right\} = \left\{\begin{array}{l} 0 \\ j\sqrt{\frac{1}{dL}}\exp(+j(k_{xm,\alpha}x)) \end{array}\right. \tag{39}$$

$$\left\{\begin{array}{c} |TEM_{\alpha}\rangle \\ m = 0 \\ n = 0 \end{array}\right\} = \left\{\begin{array}{c} |TE_{00,\alpha}\rangle \\ m = 0 \\ n = 0 \end{array}\right\} = \left\{\begin{array}{l} 0 \\ j\sqrt{\frac{1}{dL}}\exp(+j(\alpha x)) \end{array}\right. \tag{40}$$

$$\left\{\begin{array}{c} |TM_{mn,\alpha}\rangle \\ m \in Z \\ n \in N^* \end{array}\right\} = \left\{\begin{array}{l} -\frac{k_{xm,\alpha}}{\sqrt{k^2_{xm,\alpha}+k^2_{yn}}}\sqrt{\frac{2}{dL}} \\ \exp(+j(k_{xm,\alpha}x))\sin(k_{yn}y) \\ j\frac{k_{yn}}{\sqrt{k^2_{xm,\alpha}+k^2_{yn}}}\sqrt{\frac{2}{dL}} \\ \exp(+j(k_{xm,\alpha}x))\cos(k_{yn}y) \end{array}\right. \tag{41}$$

The $|TM_{m0,\alpha}\rangle$ and $|TM_{00,\alpha}\rangle$ do not exist.

$k_{xm,\alpha} = \frac{2m\pi}{d} + \alpha$ and $k_{yn} = \frac{n\pi}{L}$ are wavenumbers.

By applying the local form of Maxwell equations and verifying $\langle f_{mn,\alpha}|f_{m',n',\alpha}\rangle = \delta^{m',n'}_{m,n}$ (the Kronecker symbol), we can be sure that the new basis functions obey to: $\overrightarrow{rot}(\vec{E}) = -j\mu\omega\vec{H}$ and $\mathrm{div}(\vec{E}) = -j\beta E_z$, precisely:

$$\text{For } |TM_{mn,\alpha}\rangle \text{ the: } \left\{\begin{array}{l} H_z = 0 \\ E_z \neq 0 \end{array}\right. \Rightarrow \overrightarrow{rot}(|TM_{mn,\alpha}\rangle) = \vec{0}$$

$$\text{For } |TE_{mn,\alpha}\rangle \text{ the: } \left\{\begin{array}{l} E_z = 0 \\ H_z \neq 0 \end{array}\right. \Rightarrow \mathrm{div}(|TE_{mn,\alpha}\rangle) = 0$$

$\tilde{z}_{mn,\alpha}$, the total modal impedance associated with these vectors, can be expressed as:

$$\tilde{z}^{TE}_{mn,\alpha,upper} = \frac{j\omega\mu_0}{\gamma^2(k_{xm,\alpha},k_{yn})} \tag{42}$$

$$\tilde{z}^{TM}_{mn,\alpha,upper} = \frac{\gamma^2(k_{xm,\alpha},k_{yn})}{j\omega\epsilon_0} \tag{43}$$

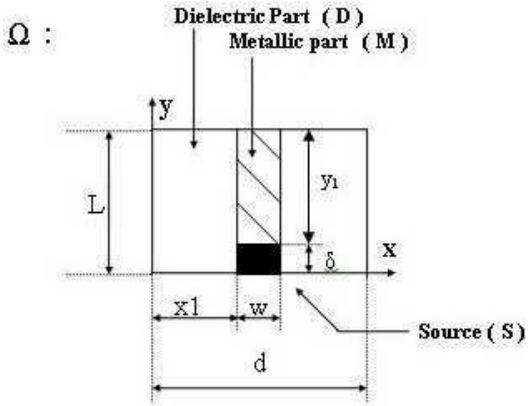

Figure 3. Discontinuity plane (Ω).

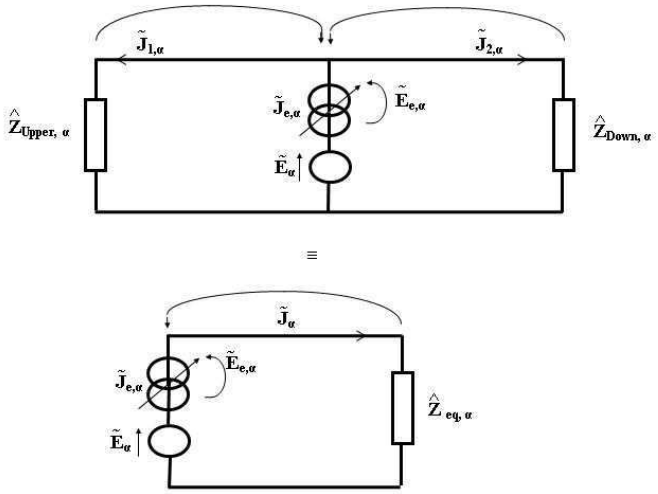

Figure 4. Equivalent circuit for unit cell.

$$\gamma^2(k_{xm,\alpha}, k_{yn}) = k_{xm,\alpha}^2 + k_{yn}^2 - k^2 \tag{44}$$

And

$$\tilde{z}_{mn,\alpha,down}^{TE} = \frac{j\omega\mu_0}{\gamma^2(k_{xm,\alpha}, k_{yn})} \tanh(\gamma(k_{xm,\alpha}, k_{yn})h) \tag{45}$$

$$\tilde{z}_{mn,\alpha,down}^{TM} = \frac{\gamma^2(k_{xm,\alpha}, k_{yn})}{j\omega\epsilon_r\epsilon_0} \tanh(\gamma(k_{xm,\alpha}, k_{yn})h) \tag{46}$$

$$\gamma^2(k_{xm,\alpha}, k_{yn}) = k_{xm,\alpha}^2 + k_{yn}^2 - \epsilon_r k^2 \tag{47}$$

$$K = 2\pi f\sqrt{\epsilon_r\epsilon_0\mu_0} \tag{48}$$

$|g_{pq,\alpha}\rangle$ designates a trial function and $I_{pq,\alpha}$ the unknown coefficients of this function to be determined.

The real source (with uniform field) $\tilde{E}_\alpha = f\tilde{V}_\alpha = \frac{1}{\delta}\tilde{V}_\alpha$ represents the excitation term associated to feeding element location connected to the radiating surface by the strip line (see Figure 3). This kind of source must also respect the property of the located element which should be smaller than the wavelength (dimensions inferior than $\frac{\lambda}{10}$) in order to introduce a neglected phase shift.

It is possible to express the excitation source by a non-uniform field, in which $\tilde{E}_\alpha = f\tilde{V}_\alpha = \frac{\tilde{V}_\alpha}{\Pi\delta}\frac{1}{\sqrt{1-(\frac{2}{\delta}(y-\frac{\delta}{2}))^2}}$ [21, 22].

The discontinuity surface can be dissociated into a metallic surface and a dielectric surface. The virtual current source $\tilde{J}_{e,\alpha}$ is defined on the metallic surface and is null on the dielectric part. We note $\tilde{E}_\alpha$ its dual.

This studied problem is modeled using the GEC method, and the circuit in Figure 4 is able to identify the relation between the electric field and the current using the impedance operator.

The development done for the unit cell leads to the expression of the input impedance for any spectral mode as stated in (49).

$$\tilde{Z_{in,\alpha}} = \left({}^t\left[\tilde{A}_\alpha\right] \left(\left[\hat{Z}_{pq,st,\alpha}^{down}\right]^{-1} + \left[\hat{Z}_{pq,st,\alpha}^{upper}\right]^{-1} \right) \left[\tilde{A}_\alpha\right] \right)^{-1} \tag{49}$$

where

$$\left[\tilde{A}_\alpha\right] = [\langle f|g_{pq,\alpha}\rangle] = \left[\left\langle \frac{1}{\delta}|g_{pq,\alpha}\right\rangle\right] \tag{50}$$

In fact, when we apply the laws of tension and current, we deduce the relation between virtual and real sources and its duals [12].

From this circuit, we can deduce the following system:

$$\tilde{J}_\alpha = \tilde{J}_{e,\alpha} \tag{51}$$

$$\tilde{E}_{e,\alpha} = \tilde{E}_\alpha + \hat{Z}_\alpha \tilde{J}_{e,\alpha} \tag{52}$$

In this case, the used waveguide is the EPEP guide. We are interested in the study of the input impedance for each mode in spectral domain, and we can deduce the current densities lying in metal part including the source domain to verify the boundary conditions.

Next, the integral equation is solved on the central element by applying the MoM method using Galerkin procedure. Taking into account that the original periodic excitation is written as a combination of Floquet-periodic impressed fields by means of the linear transformation in (11), (15), after applying the superposition principle, the current density excited by the located source on the periodic micro-strip line can be finally computed as [3, 9, 17]:

$$J(x,y) = \frac{d}{2\pi} \int_{\frac{-\pi}{d}}^{\frac{\pi}{d}} \tilde{J}_\alpha(x,y)\, d\alpha \tag{53}$$

Similarly, we express the superposition theorem:

$$J(x,y) = \frac{1}{\sqrt{N_x}} \sum_p \tilde{J}_{\alpha_p}(x,y) \tag{54}$$

3.2. Spatial Formulation

Secondly, this case will be studied separately and corresponds to global structure (reference structure). Generally, using this direct manner, which employs a spatial formulation to calculate an integral-equation (IE), permits to deduce the mutual relationships that can be computed by an impedance matrix [6] and compared with others obtained by simple transformation (FFT) explained in relation (32).

Next, N_x uniform and identical sources will excite respectively every strip-line that belongs to the whole array configuration (also non-uniform with distinct amplitude of these sources can be treated).

These sources are called located elements which have neglected dimensions compared with the guide's wavelength λ_g. The MoM-GEC approach consists of Maxwell equations and the continuity relations with generalized equivalent circuit model [5, 18–20, 26]. Their generalized equivalent circuits are shown in Figure 5.

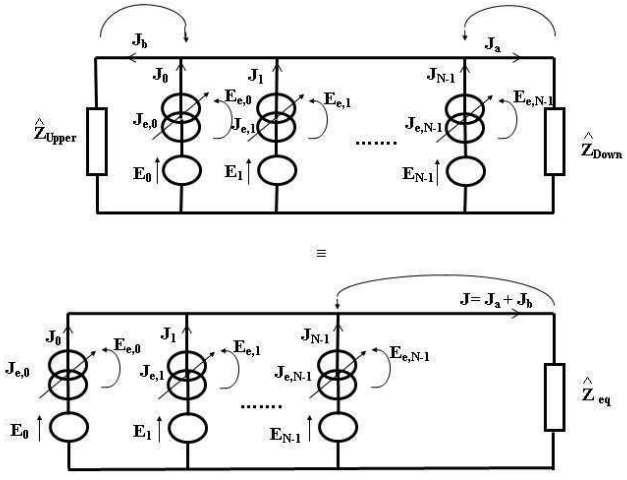

Figure 5. Equivalent circuit for global structure.

Let $|f_{mn}^{TE,TM}\rangle$ be the modes (or basis functions) of the proposed waveguide enclosing the studied structure (see Figure 1).

The excitation fields E_i, $i \in [0, N-1]$ are expressed as follows $E_i = V_i f_i$ where $f_i = \frac{1}{\delta}$ represents the fundamental excitations modes.

The impedance operator $\hat{Z}$ is expressed as the function of higher-order modes and their modes impedances $z_{mn}^{TE,TM}$. The unknown of the problem J_e^i describes the virtual current appearing on each metal part and represents the electromagnetic state on the discontinuity interface.

So J_e^i is expressed as a series of known test functions g_{pq}^i weighted by unknown coefficients.

Based on its corresponding equivalent circuit model depicted in Figure 5, the generalized Ohm and Kirchhoff laws are then rewritten as equations system:

$$\begin{cases} J_i = J_{e,i} \\ E_{e,i} = E_i + \hat{Z} J \end{cases} \tag{55}$$

with:

$$J = J_{e,0} + J_{e,1} + \ldots + J_{e,N-1} = J_0 + J_1 + \ldots + J_{N-1} \tag{56}$$

A formal relation between sources (real and virtual) and their duals is given in (57):

$$\left(\begin{array}{c} J_0 \\ . \\ . \\ J_{N-1} \\ \hline E_{e,0} \\ . \\ . \\ E_{e,N-1} \end{array}\right) = \left(\begin{array}{cccc|cccc} 0 & . & . & 0 & 1 & 0 & . & 0 \\ 0 & . & . & 0 & 0 & 1 & 0 & . \\ 0 & . & . & 0 & . & 0 & 1 & 0 \\ 0 & . & . & 0 & 0 & . & 0 & 1 \\ \hline 1 & 0 & . & 0 & & & & \\ 0 & 1 & 0 & . & & & & \\ . & 0 & 1 & 0 & & \hat{Z_{pq,st}} & & \\ 0 & . & 0 & 1 & & & & \end{array}\right) \left(\begin{array}{c} E_0 \\ . \\ . \\ E_{N-1} \\ \hline J_{e,0} \\ . \\ . \\ J_{e,N-1} \end{array}\right) \tag{57}$$

After that, we apply the Galerkin procedure to Equation (57). Consequently, the impedance matrix $Z_{i,j}$ of the total structure (multiport microwave circuits) is as following:

$$[Z_{i,j}] = \left[\frac{V_i}{I_j}\right] = \left({}^t[A] \left(\left[\hat{Z}_{pq,st}^{down}\right]^{-1} + \left[\hat{Z}_{pq,st}^{upper}\right]^{-1}\right)[A]\right)^{-1} \tag{58}$$

where: $[A] = [\langle f_i | g_{pq,st}^i \rangle]$, $[\hat{Z_{pq,st}}] = [\langle g_{pq}^i | \hat{Z} | g_{st}^j \rangle]$, $(i,j) \in [0, N-1][0, N-1]$ and $\hat{Z} = \sum_{m,n} |f_{mn}^{TE,TM}\rangle z_{mn,TE,TM}^{upper,down} \langle f_{mn}^{TE,TM}|$. Therefore, the mutual coupling effects in this case are expressed with the driving impedance matrix.

As Equation (58) relates these voltages V_i and currents I_j in the passive impedance case, the matrix representation is written as:

$$[Z][I] = [V] \tag{59}$$

Identically, the admittance matrix, $[Y_{i,j}]$, is simply the inverse of the impedance matrix $[Z_{i,j}]$.

$$[Y_{i,j}] = [Z_{i,j}]^{-1} \tag{60}$$

From (59) we see that $Z_{i,j}$ can be found as:

$$Z_{i,j} = \left.\frac{V_i}{I_j}\right|_{I_k = 0 (\text{for } k \neq j)} \tag{61}$$

Briefly, (59) states that $Z_{i,j}$ can be found by driving port j with the current I_j, open-circuiting all other excitations $I_k = 0$ (for $k \neq j$), and measuring the open circuit voltage at port i. In addition, $Z_{i,i}$ is the

input impedance looking into source i when all other sources are open-circuited, and $Z_{i,j}$ is the transfer impedance between excitation sources i and j when all other excitations are open circuited.

The same from $Y_{i,j}$ can be found as:

$$Y_{i,j} = \left.\frac{I_i}{V_j}\right|_{V_k=0(\text{for } k\neq j)} \tag{62}$$

which states that $Y_{i,j}$ can be found by driving port j with the current V_j, short-circuiting all other excitations $V_k = 0$ (for $k \neq j$), and measuring the open circuit voltage at port i. In addition, $Y_{i,i}$ is the input impedance looking into port i when all other ports are short-circuited.

The scattering parameter corresponding to the unique impedance matrix is written in the following form:

$$[S_{i,j}] = \left[\frac{Z_{i,j}}{Z_c} - I\right]\left[\frac{Z_{i,j}}{Z_c} + I\right]^{-1} \tag{63}$$

where Z_c is also the desired reference impedance of each element. For example, if the matrix is re-normalized to 50 ohms, then (Z_c) will have values of $50\,\Omega$.

Relations (55) and (56) allow us to calculate the current densities lying in metal parts and their associated fields including the sources domains to verify the suggested boundary conditions.

Following this formulation, it is possible to study the edge effects along the x direction where walls can be modified or displaced and to show the surface waves [24] and their supporting role by changing the separation distance between elements especially in strong coupling cases (or in aperiodic representation where only central element can be excited and the others no-excited elements).

4. NUMERICAL RESULTS

Let us consider the structure given in Figure 2 to calculate the input impedance for each mode (spectral input impedance) using the Galerkin's procedure: After studying the convergence for this input impedance against the basis functions number, when the sinusoidal test functions number describing the metal part is fixed to 40, the following result is obtained as shown in Figure 6.

It is noted that the method of moments converges quickly towards the solution, since the convergence level appears beyond 90000 (300×300) basis functions.

A good convergence study is elaborated to investigate the theoretical input impedance Z_{in} evaluated by the MoM-GEC for one unit cell in 1-D-periodic micro strip array.

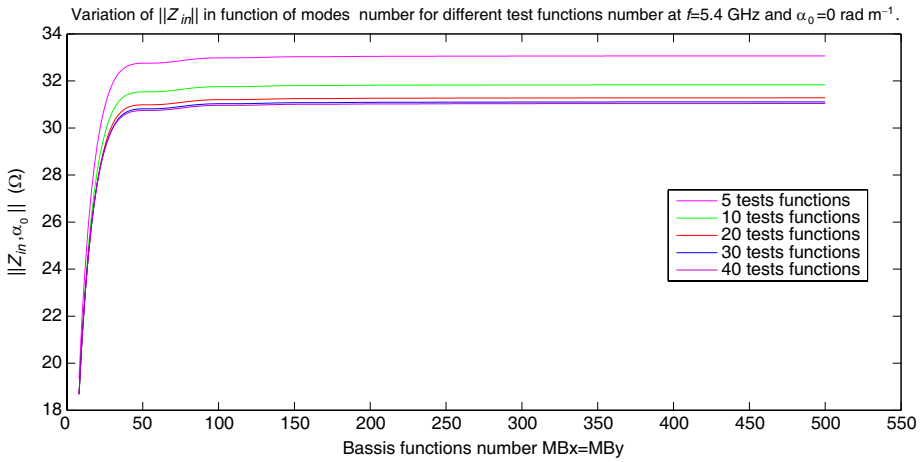

Figure 6. Variation of $\|Z_{in,\alpha_0}\|$ in function of the guide's modes number for different test functions number at $f = 5.4\,\text{GHz}$ and $\alpha_0 = 0\,\text{rad m}^{-1}$. The parameters which chosen to simulate the suggested unit structure are: $w = 1\,\text{mm}$, $\delta = 0.75\,\text{mm}$ ($w \ll \lambda_0$, $\delta \ll \lambda_0$), $d \approx \lambda_0 \approx 54\,\text{mm}$, $L = \lambda_0 \approx 54\,\text{mm}$, $h = 1.25\,\text{mm}$ and $\epsilon_r = \epsilon_0 = 1$ (air).

We observe in Figure 6 that convergence criteria of the employed method (modal method) based on moment's method should be achieved in 90000 (300×300) basis functions.

Figures 7 and 8 depict the real and the imaginary parts of Z_{in} against frequency for different test functions.

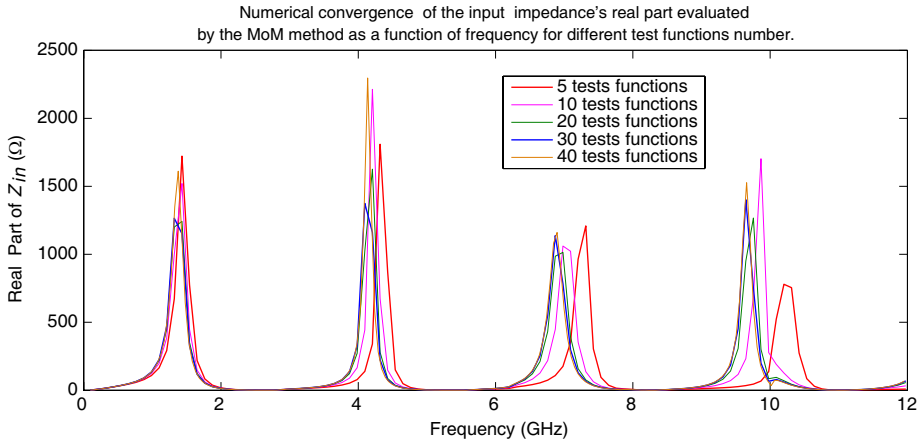

Figure 7. Numerical convergence of the input impedance's real part evaluated by the MoM method as a function of frequency for different test functions number: $\alpha_0 = 0\,\text{rad m}^{-1}$, $w = 1\,\text{mm}$, $\delta = 0.75\,\text{mm}$ ($w \ll \lambda_0,\ \delta \ll \lambda_0$), $d \approx \lambda_0 \approx 54\,\text{mm}$, $L = \lambda_0 \approx 54\,\text{mm}$, $h = 1.25\,\text{mm}$ and $\epsilon_r = \epsilon_0 = 1$ (air).

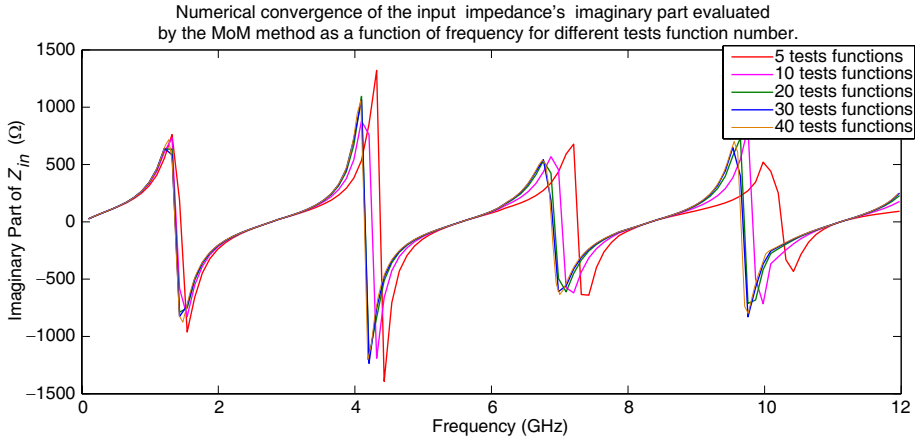

Figure 8. Numerical convergence of the input impedance's imaginary part evaluated by the MoM method as a function of frequency for different test functions number: $\alpha_0 = 0\,\text{rad m}^{-1}$, $w = 1\,\text{mm}$, $\delta = 0.75\,\text{mm}$ ($w \ll \lambda_0,\ \delta \ll \lambda_0$), $d \approx \lambda_0 \approx 54\,\text{mm}$, $L = \lambda_0 \approx 54\,\text{mm}$, $h = 1.25\,\text{mm}$ and $\epsilon_r = \epsilon_0 = 1$ (air).

Impedance Z_{in} observed by the excitation source is calculated for the frequencies between 0–12 GHz to justify the electromagnetic quantity in (49) (taking the particular case $\alpha_0 = 0$). The same study can be extended for $\alpha_p \neq 0$.

The behavior of Z_{in} as a function of frequency allows determining the resonance frequency of the studied structure. These frequencies are in good agreement with electromagnetic theory that between two distinct resonances, we should assure a difference equal to $\frac{\lambda_0}{2} \approx 27\,\text{mm}$.

Figure 9 indicates that the impedance will be allowed imaginary regardless the line length. The impedance Z_{in} varies between $-j\infty$ and $+j\infty$. At $y = 0$, the input impedance is $Z_{in} = 0$, whereas at $y = \frac{\lambda_0}{4}$, $Z_{in} = \infty$. The strip line transforms the short-circuit in an open circuit in which reflexion coefficient at the load is $\Gamma_L = -1$. The input impedance is capacitive and inductive every quarter wave length.

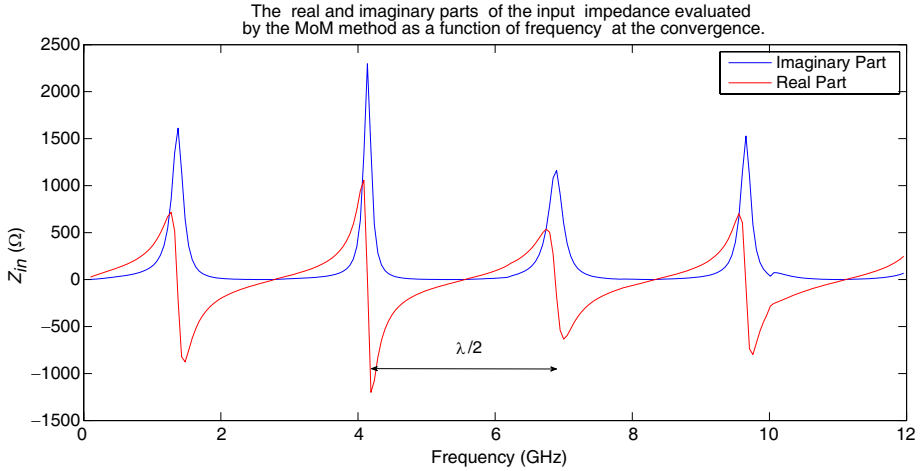

Figure 9. Evolution of the real and imaginary parts of input impedance evaluated by the MoM method against the frequency at the convergence: $\alpha_0 = 0\,\text{rad m}^{-1}$, $w = 1\,\text{mm}$, $\delta = 0.75\,\text{mm}$ ($w \ll \lambda_0,\ \delta \ll \lambda_0$), $d \approx \lambda_0 \approx 54\,\text{mm}$, $L = \lambda_0 \approx 54\,\text{mm}$, $h = 1.25\,\text{mm}$ and $\epsilon_r = \epsilon_0 = 1$ (air).

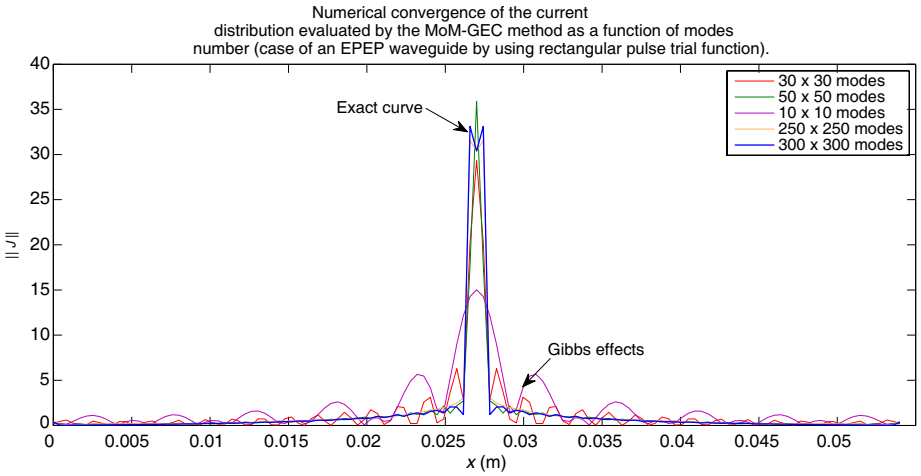

Figure 10. Numerical convergence of current distribution's magnitude ($\frac{A}{m}$) evaluated by the MoM method as a function of basis functions number at $f = 5.4\,\text{GHz}$ and $\alpha_0 = 0\,\text{rad m}^{-1}$ (Rectangular pulse trial functions) (case of an EPEP waveguide): $w = 1\,\text{mm}$, $\delta = 0.75\,\text{mm}$ ($w \ll \lambda_0,\ \delta \ll \lambda_0$), $d \approx \lambda_0 \approx 54\,\text{mm}$, $L = \lambda_0 \approx 54\,\text{mm}$, $h = 1.25\,\text{mm}$ and $\epsilon_r = \epsilon_0 = 1$ (air).

The strip line behaves as inductance for little shape circuits, with low inductance values. We may use a line ending by short-circuit.

Thus, for better understanding these results, we propose to study this convergence with another manner based on the current density in function of the basis functions number.

Figures 10 and 11 represent the current behavior as a function of the basis functions number using two different suggested trial functions: Rectangular pulse function and U trial function (Rectangular pulse function weighted by $(\sqrt{1-(\frac{2}{w}(x-\frac{d-w}{2}))^2})$ along the x direction dependence. It is shown that the current convergence is obtained for 300 basis functions in which the Gibbs effects are practically suppressed, and these oscillations resulting from truncation are due to the Gibbs phenomenon. Because of this effect, we cannot write the boundary conditions in the immediate neighbourhood of the metal-dielectric plane [25].

Figures 16 and 17 illustrate that the current evaluated by the MoM and obtained at convergence conforms to the theory with consideration to the boundary conditions.

Based on this current representation in the unit cell, it is observed that it is considerably possible

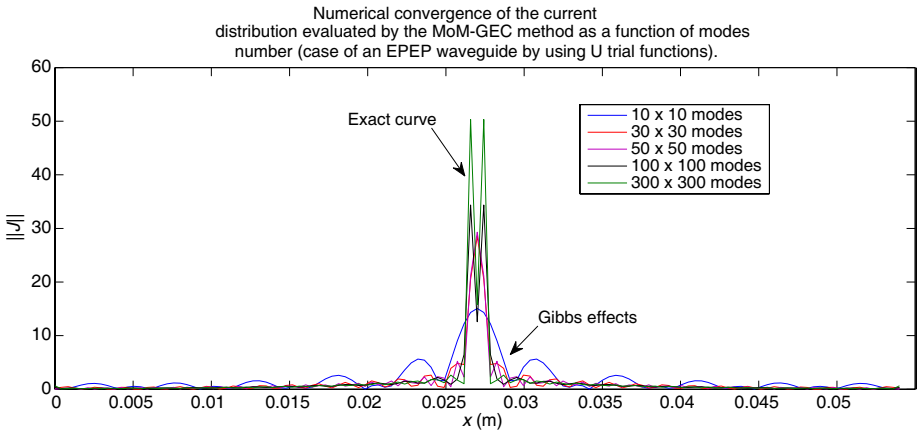

Figure 11. Numerical convergence of current distribution's magnitude ($\frac{A}{m}$) evaluated by the MoM method as a function of basis functions number at $f = 5.4\,\text{GHz}$ and $\alpha_0 = 0\,\text{rad m}^{-1}$ (U trial functions) (case of an EPEP waveguide): $w = 1\,\text{mm}$, $\delta = 0.75\,\text{mm}$ ($w \ll \lambda_0$, $\delta \ll \lambda_0$), $d \approx \lambda_0 \approx 54\,\text{mm}$, $L = \lambda_0 \approx 54\,\text{mm}$, $h = 1.25\,\text{mm}$ and $\epsilon_r = \epsilon_0 = 1$ (air).

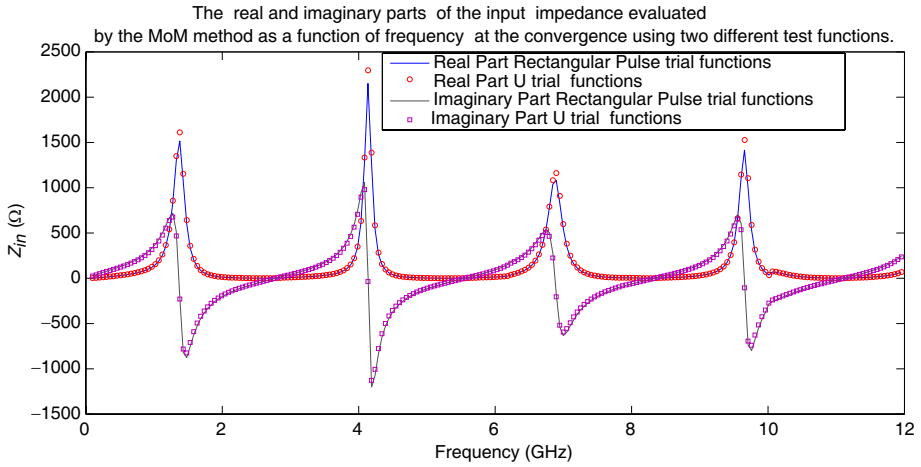

Figure 12. The real and imaginary parts of the input impedance evaluated by the MoM method against the frequency at the convergence using two different test functions (dependence in x direction): $\alpha_0 = 0\,\text{rad m}^{-1}$, $w = 1\,\text{mm}$, $\delta = 0.75\,\text{mm}$ ($w \ll \lambda_0$, $\delta \ll \lambda_0$), $d \approx \lambda_0 \approx 54\,\text{mm}$, $L = \lambda_0 \approx 54\,\text{mm}$, $h = 1.25\,\text{mm}$ and $\epsilon_r = \epsilon_0 = 1$ (air).

to identify spatial case with the same manner that the current distributions in Figures 18 and 19 verify the boundary conditions where walls are EPEP (with null phases shift) in the reference structure.

All results obtained in Figure 10 and Figure 6 prove that the convergence level corresponding to spectral input impedance and current density is identically associated to (300) basis functions (otherwise for 90000 (300×300) basis functions number).

According to Figure 12, the variation of the test function's dependence in x direction by using pulse functions or weighted pulse functions (U trial functions) keeps the same response.

Figure 13 draws the magnitude of the input impedance evaluated by the MoM method against the frequency at the convergence using two different source fields, which proves the identical behavior but not the same values because of the expression of the located element's fundamental excitation field which take effects on the excitation vector's components. We have to note that the source is badly matched in our case because it is not independent of these applied fields.

Figure 14 represents the magnitude's numerical value of the input impedance behavior against the frequency for different discrete spectral values in finite case composed of 4 elements in periodic array.

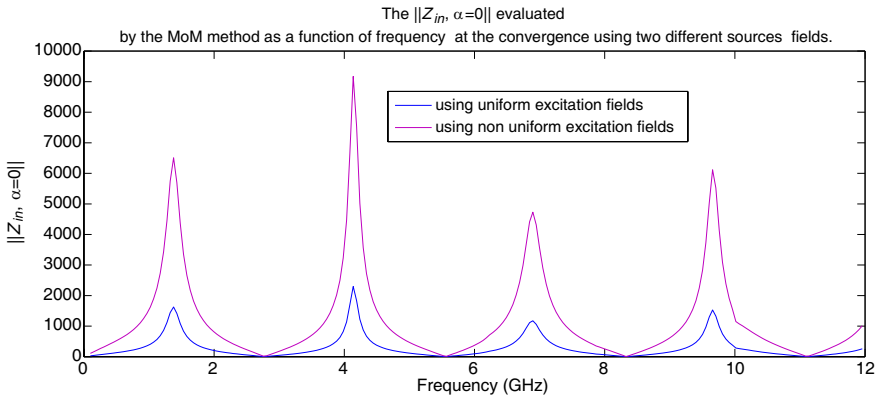

Figure 13. The magnitude of the input impedance evaluated by the MoM method against the frequency at the convergence using two different source fields: $\alpha_0 = 0\,\text{rad m}^{-1}$, $w = 1\,\text{mm}, \delta = 0.75\,\text{mm}$ $(w \ll \lambda_0,\ \delta \ll \lambda_0)$, $d \approx \lambda_0 \approx 54\,\text{mm}$, $L = \lambda_0 \approx 54\,\text{mm}$, $h = 1.25\,\text{mm}$ and $\epsilon_r = \epsilon_0 = 1$ (air).

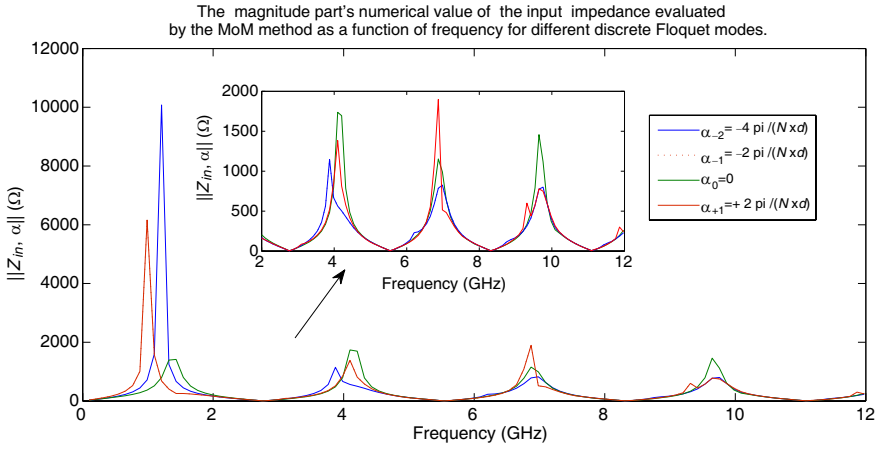

Figure 14. The magnitude part's numerical value of the input impedance evaluated by the MoM method as a function of frequency for different discret Floquet modes: $w = 1\,\text{mm}$, $\delta = 0.75\,\text{mm}$ $(w \ll \lambda_0,\ \delta \ll \lambda_0)$, $d \approx \lambda_0 \approx 54\,\text{mm}$, $L = \lambda_0 \approx 54\,\text{mm}$, $h = 1.25\,\text{mm}$ and $\epsilon_r = \epsilon_0 = 1$ (air).

The Floquet-input impedance shows the symmetry property especially in our case when the curves corresponding to $Z_{in,\alpha_{-1}}$ and $Z_{in,\alpha_{+1}}$ are conformed [7]. Then the edge effects are neglected.

Also the obtained result in Figure 14 shows that the mutual couplings are strong between elements only at the resonances which contain distinct values of the modal impedances, whereas along the rest of frequencies there is a weak coupling.

If the identical cells are not coupled especially when the spatial period $(d \geq \lambda_0)$, the values of $Z_{in,\alpha}$ are practically constant and independent of α because the source is not sensitive to the boundary of each cell. Consequently, it appears that the $[\tilde{z}_{\alpha_p}]$ matrix is diagonal with identical terms. But, in our case to take into account mutual parameters in strong coupling, we should have a spatial period $(d \ll \lambda_0)$ for example $(d \approx \frac{\lambda_0}{4})$ which permits modal input impedance to depend on appreciably modal states (Floquet's modes).

According to the following study we define Table 1 which contains the possible spectral values (Finite structure) of input impedance at $f = 5.4\,\text{GHz}$.

Table 1 permits to deduce the mutual coupling parameters by using spectral representation: To validate this work, a good agreement with spatial method is shown in the scattering coupling parameters, and practically the $[S]$ matrix has the same values when elements are strongly or weakly coupled, as shown in Tables 2 and 3. Then, the maximum residual error between scattering coupling parameters

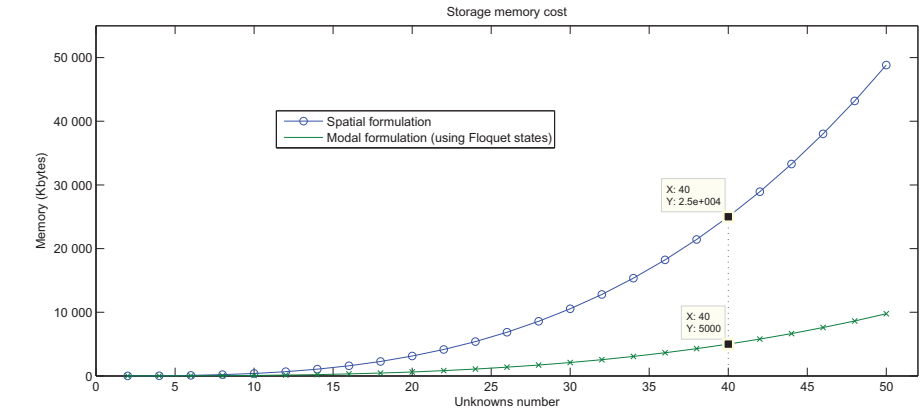

(a) Storage memory cost.

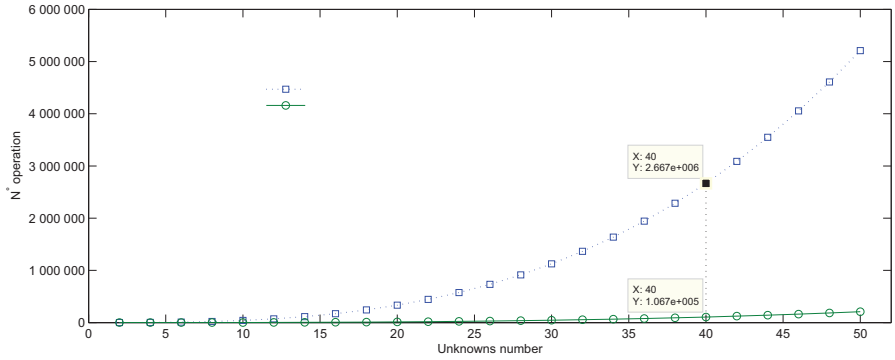

(b) Computational cost.

Figure 15. Computational cost versus the number of unknowns.

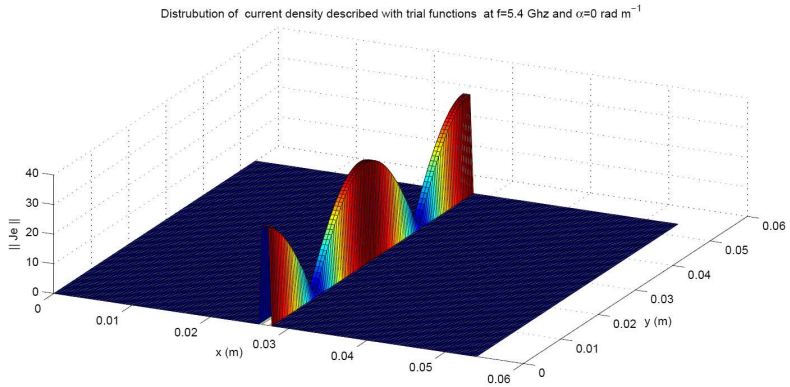

Figure 16. 2-D representation of the current density ($\frac{A}{m}$) described with trial functions (Rectangular pulse trial functions) at $f = 5.4\,\text{GHz}$ and $\alpha_0 = 0\,\text{rad m}^{-1}$: $w = 1\,\text{mm}$, $\delta = 0.75\,\text{mm}$ ($w \ll \lambda_0$, $\delta \ll \lambda_0$), $d \approx \lambda_0 \approx 54\,\text{mm}$, $L = \lambda_0 \approx 54\,\text{mm}$, $h = 1.25\,\text{mm}$ and $\epsilon_r = \epsilon_0 = 1$ (air).

can be attained, in this case 3.2364%.

To confirm our result, we try to choose another operating frequency, for example at the resonance where $f \simeq 4\,\text{GHz}$. Also a good correspondence between spatial and spectral (modal) formulation is obtained, and the maximum residual value is about 9.2364%. By using HFSS simulation tools, we have also generated the $[S]$ matrix of the global structure that practically reinforces our results given by both the formulations, as illustrated in Tables 6, 7, and 8 (same in Tables 2, 3, and 4). Concerning the

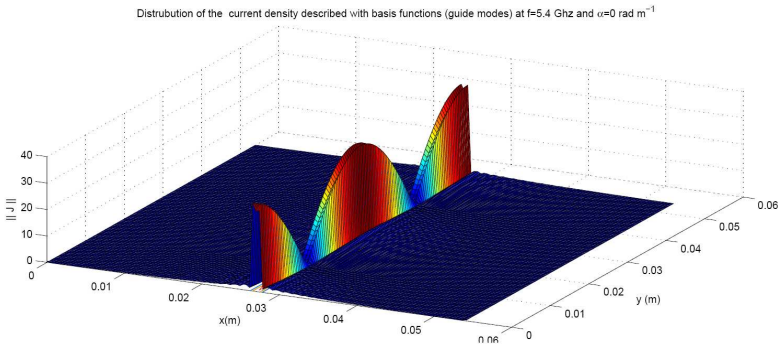

Figure 17. 2-D representation of the current density ($\frac{A}{m}$) described with guide's modes at $f = 5.4\,\text{GHz}$ and $\alpha_0 = 0$ rad m^{-1}: $w = 1\,\text{mm}$, $\delta = 0.75\,\text{mm}$ ($w \ll \lambda_0,\ \delta \ll \lambda_0$), $d \approx \lambda_0 \approx 54\,\text{mm}$, $L = \lambda_0 \approx 54\,\text{mm}$, $h = 1.25\,\text{mm}$ and $\epsilon_r = \epsilon_0 = 1$ (air).

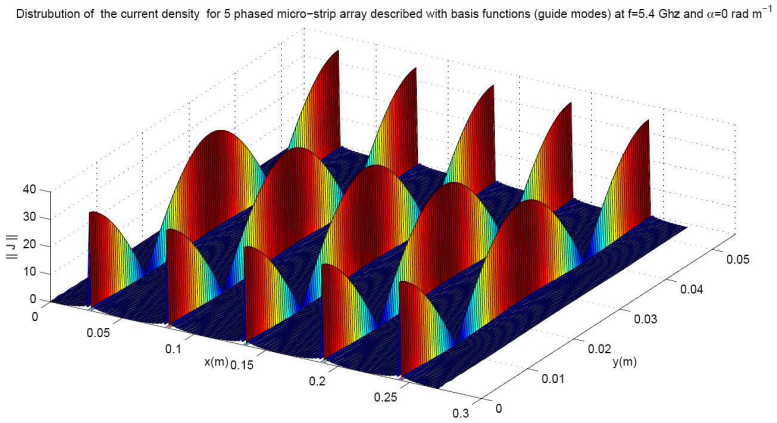

Figure 18. 2-D representation of the current density ($\frac{A}{m}$) for 5 phased micro-strip array described with basis functions (guide's modes) at $f = 5.4\,\text{GHz}$ and $\alpha_0 = 0\,\text{rad m}^{-1}$: $w = 1\,\text{mm}$, $\delta = 0.75\,\text{mm}$ ($w \ll \lambda_0,\ \delta \ll \lambda_0$), $d \approx \lambda_0 \approx 54\,\text{mm}$, $L = \lambda_0 \approx 54\,\text{mm}$, $a = 270\,\text{mm}$, $h = 1.25\,\text{mm}$ and $\epsilon_r = \epsilon_0 = 1$ (air).

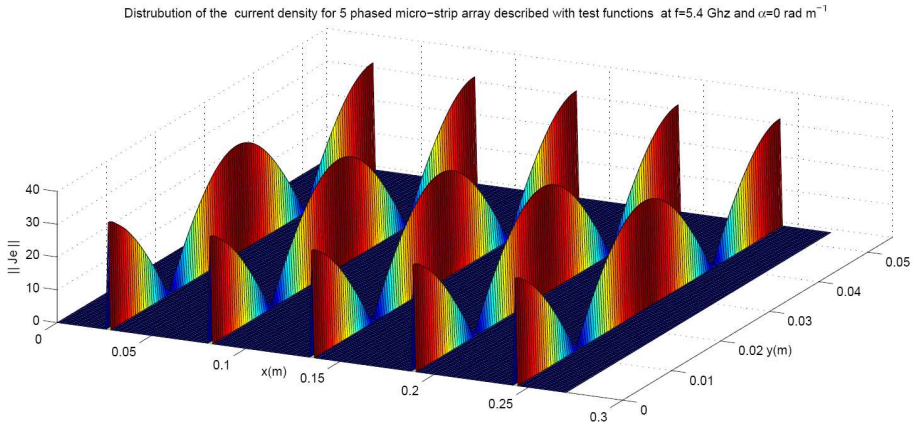

Figure 19. 2-D representation of the current density ($\frac{A}{m}$) for 5 phased micro-strip array described with trial functions (Rectangular pulse trial functions) at $f = 5.4\,\text{GHz}$ and $\alpha_0 = 0\,\text{rad m}^{-1}$: $w = 1\,\text{mm}$, $\delta = 0.75\,\text{mm}$ ($w \ll \lambda_0,\ \delta \ll \lambda_0$), $d \approx \lambda_0 \approx 54\,\text{mm}$, $L = \lambda_0 \approx 54\,\text{mm}$, $a = 270\,\text{mm}$, $h = 1.25\,\text{mm}$ and $\epsilon_r = \epsilon_0 = 1$ (air).

Table 1. Spectral input impedance at $f = 5.4\,\text{GHz}$ (finite case): $w = 1\,\text{mm}$, $\delta = 0.75\,\text{mm}$ ($w \ll \lambda_0,\ \delta \ll \lambda_0$), $d \approx \frac{\lambda_0}{4} \approx 4\,\text{mm}$, $L = \lambda_0 \approx 54\,\text{mm}$, $N_x = 5$ elements, $h = 1.25\,\text{mm}$ and $\epsilon_r = \epsilon_0 = 1$ (air).

p	-2	-1	0	$+1$	$+2$
α_p (rad m^{-1})	$\frac{-4pi}{N_x d}$	$\frac{-2pi}{N_x d}$	0	$\frac{+2pi}{N_x d}$	$\frac{+4pi}{N_x d}$
Z_{in,α_p} (Ω)	0–23.9556i	0–27.2179i	0.9651–38.7581i	0–27.2179i	0–23.9556i

Table 2. Mutual coupling parameters S_{ij} (dB) between the center element and other elements obtained using spectral formulation (or modal representation based on Floquet's modes) at $f = 5.4\,\text{GHz}$: $w = 1\,\text{mm}$, $\delta = 0.75\,\text{mm}$, ($w \ll \lambda_0,\ \delta \ll \lambda_0$), $d \approx \frac{\lambda_0}{4} \approx 4\,\text{mm}$, $L = \lambda_0 \approx 54\,\text{mm}$, $N_x = 5$ elements, $h = 1.25\,\text{mm}$, $Z_c = 50\,\Omega$ and $\epsilon_r = \epsilon_0 = 1$ (air).

-0.1465	-20.3464	-25.7783	-25.7783	-20.3464
-20.3464	-0.1465	-20.3464	-25.7783	-25.7783
-25.7783	-20.3464	$\boxed{-0.1465}$	-20.3464	-25.7783
-25.7783	-25.7783	-20.3464	-0.1465	-20.3464
-20.3464	-25.7783	-25.7783	-20.3464	-0.1465

Table 3. Mutual coupling parameters S_{ij} (dB) between the center element and other elements obtained using spatial formulation at $f = 5.4\,\text{GHz}$ and $\alpha_0 = 0\,\text{rad m}^{-1}$: $w = 1\,\text{mm}$, $\delta = 0.75\,\text{mm}$, ($w \ll \lambda_0,\ \delta \ll \lambda_0$), $d \approx \frac{\lambda_0}{4} \approx 4\,\text{mm}$, $a = 20\,\text{mm}$, $L = \lambda_0 \approx 54\,\text{mm}$, $N_x = 5$ elements, $h = 1.25\,\text{mm}$, $Z_c = 50\,\Omega$ and $\epsilon_r = \epsilon_0 = 1$ (air).

-0.1514	-20.0143	-26.1074	-26.1074	-20.0143
-20.0143	-0.1514	-20.0143	-26.1074	-26.1074
-26.1074	-20.0143	$\boxed{-0.1514}$	-20.0143	-26.1074
-26.1074	-26.1074	-20.0143	-0.1514	-20.0143
-20.0143	-26.1074	-26.1074	-20.0143	-0.1514

Table 4. Mutual coupling parameters S_{ij} (dB) between the center element and other elements obtained using HFSS (reference structure) at $f = 5.4\,\text{GHz}$.

-0.1467	-24.1908	-29.8150	-29.8150	-24.1908
-24.1908	-0.1467	-24.1908	-29.8150	-29.8150
-29.8150	-24.1908	$\boxed{-0.1467}$	-24.1908	-29.8150
-29.8150	-29.8150	-24.1908	-0.1467	-24.1908
-24.1908	-29.8150	-29.8150	-24.1908	-0.1467

Table 5. Spectral input impedance at $f = 4\,\text{GHz}$ (finite case): $w = 1\,\text{mm}$, $\delta = 0.75\,\text{mm}$ ($w \ll \lambda_0,\ \delta \ll \lambda_0$), $d \approx \frac{\lambda_0}{4} \approx 4\,\text{mm}$, $L = \lambda_0 \approx 54\,\text{mm}$, $N_x = 5$ elements, $h = 1.25\,\text{mm}$ and $\epsilon_r = \epsilon_0 = 1$ (air).

p	-2	-1	0	$+1$	$+2$
α_p (rad m^{-1})	$\frac{-4pi}{N_x d}$	$\frac{-2pi}{N_x d}$	0	$\frac{+2pi}{N_x d}$	$\frac{+4pi}{N_x d}$
Z_{in,α_p} (Ω)	$0 + 762i$	$0 + 1515.2i$	$1181.5 - 457.2i$	$0 + 1515.2i$	$0 + 762i$

values of $S_{11}(db)$, they are always poor due to the nature of the chosen motif which is short-circuited and attached to the ground plane that permits to emit a maximum of radiating power when the transfer power between elements is assured.

Table 6. Mutual coupling parameters S_{ij} (dB) between the center element and other elements obtained using spectral formulation (or modal representation based on Floquet's modes) at $f = 4\,\text{GHz}$: $w = 1\,\text{mm}$, $\delta = 0.75\,\text{mm}$ ($w \ll \lambda_0$, $\delta \ll \lambda_0$), $d \approx \frac{\lambda_0}{4} \approx 4\,\text{mm}$, $L = \lambda_0 \approx 54\,\text{mm}$, $N_x = 5$ elements, $h = 1.25\,\text{mm}$, $Z_c = 50\,\Omega$ and $\epsilon_r = \epsilon_0 = 1$ (air).

−0.1387	−27.7113	−34.8966	−34.8983	−27.7113
−27.7113	−0.1387	−27.7113	−34.8966	−34.8966
−34.8966	−27.7113	**−0.1387**	−27.7113	−34.8966
−34.8966	−34.8966	−27.7113	−0.1387	−27.7113
−27.7113	−34.8966	−34.8966	−27.7113	−0.1387

Table 7. Mutual coupling parameters S_{ij} (dB) between the center element and other elements obtained using spatial formulation at $f = 4\,\text{GHz}$ and $\alpha_0 = 0\,\text{rad m}^{-1}$: $w = 1\,\text{mm}$, $\delta = 0.75\,\text{mm}$ ($w \ll \lambda_0$, $\delta \ll \lambda_0$), $d \approx \frac{\lambda_0}{4} \approx 4\,\text{mm}$, $a = 20\,\text{mm}$, $L = \lambda_0 \approx 54\,\text{mm}$, $N_x = 5$ elements, $h = 1.25\,\text{mm}$, $Z_c = 50\,\Omega$ and $\epsilon_r = \epsilon_0 = 1$ (air).

−0.1424	−27.5240	−31.7869	−31.7869	−27.5240
−27.5240	−0.1424	−27.5240	−31.7869	−31.7869
−31.7869	−27.5240	**−0.1424**	−27.5240	−31.7869
−31.7869	−31.7869	−27.5240	−0.1424	−27.5240
−27.5240	−26.1074	−31.7869	−27.5240	−0.1424

Table 8. Mutual coupling parameters S_{ij} (dB) between the center element and other elements obtained using HFSS (reference structure) at $f = 4\,\text{GHz}$.

−0.1031	−28.8177	−36.5132	−36.5132	−28.8177
−228.8177	−0.1031	−28.8177	−34.8966	−36.5132
−36.5132	−28.8177	**−0.1031**	−28.8177	−36.5132
−36.5132	−36.5132	−28.8177	−0.1031	−28.8177
−28.8177	−36.5132	−36.5132	−28.8177	−0.1031

Following Tables 1 and 5 concerning the α value, Floquet harmonics may appear as an evanescent or propagating waves [23] which engender a scan blindness phenomena. This explains why for $\alpha = 0$, Z_{in} is a complex value, and for others α values Z_{in} is pure imaginary.

5. STORAGE MEMORY AND TIME COMPUTATION

In this section, we explain the main advantage to favor using spectral formulation other than spatial formulation in storage memory cost and reducing computational time.

In general, in order to seek for coupling parameters, the MoM-method requires $(M \times M)$ matrix inversion. We denote M as number of used trial functions (discretization functions). Hence, the memory requirement and operation number of conventional MoM depend on M as:

$$\begin{aligned} \text{Storage} &\approx O\left(M^2\right) \\ N \text{ operation} &\approx O\left(M^3\right) \end{aligned} \tag{64}$$

In consequence, the use of the direct method resting on that moment's method needs $(N_x M)^2$ memory size with N_x the number of the array elements. In modal formulation, the token $[\tilde{z}_{\alpha_p}]$ has a $N_x(M)^2$ memory size with N_x the number of the possible phases shift α_p (finite case).

However, the numerical complexity of the proposed method is restraint to spectral formulation (global matrix $[\tilde{z}_{\alpha_p}]$ calculation). In fact, the second operation (see Equations (32), (33) and (34)) permits to transform modal domain to spatial one by a simple matrix multiplication.

Finally, by reducing $[Z]$ matrix, not only its computational time will be reduced, but also the computational time of the inverse matrix will be reduced [12, 27].

According to this study, the application of the proposed procedure was applied to a 5-element array. In Figure 15, when the unknowns number increases, the operation number will increase exponentially using the spatial formulation. In addition, the manipulated matrix requires a huge memory resources when unknowns grow up. But, in spectral formulation these memory resources and operation number can be minimized greatly. That is why we prefer rather to choose Floquet analysis with spectral representation to treat large finite array or infinite array which themselves contain a large number of unknowns that must be reduced.

6. CONCLUSION

This work contains an efficient original modal analysis by introducing a new method to decompose excitation source in spectral domain according a finite and infinite periodic structures that remove the complexity of the problem under consideration to model and analyze the periodic problem when elements are strongly or weakly coupled.

Several advantages are shown for modeling periodic circuits, for example:

- The reduction of electromagnetic calculation: Instead of studying the whole array structure, the modeling of unit cell makes it possible to reduce all wave phenomena associated with the periodic structure on one unit cell (central cell).
- The reduction of computational time and storage memory for a large finite structure.
- This new modal analysis uses the direct application of Floquet's theorem by varying all spectral modes to facilitate the attack of the whole structure by a simple transformation (theorem of superposition) (in other cases named Fourier Transformation).

This study remains successfully valid for several geometries of radiating planar dipoles in various periodic or quasi-periodic configurations: That is why we propose another paper to study the mutual coupling parameters between elements in aperiodic configuration and their effects by using all this spectral formulation.

After studying the one-dimensional case, it is rather easy to study a high-dimensional case especially for finite number of planar dipoles.

REFERENCES

1. Hamdi, B., T. Aguili, and H. Baudrand, "Uni-dimensional planar almost periodic structures analysis to decompose central arbitrary located source in spectral domain," *IEEE-ANTEM 2012: 15th International Symposium of Antenna Technology and Applied Electromagnetics*, 1–5, Toulouse, France, 2012.
2. Ishimaru, A., R. J. Coe, G. E. Miller, and W. P. Green, "Finite periodic structure approach to large scanning array problems," *IEEE Trans. Antennas Propagat.*, 1213–1220, 1985.
3. Mekkioui, Z. and H. Baudrand, "Bi-periodic centered-fed microstrip leaky-wave antenna (LWA) analysis by a source modal decomposition in spectral domain," *IET*, 1141–1149, 2009.
4. Baudrand, H., M. Titaouine, N. Raveu, and G. Fontgland, "Electromagnetic modeling of planar almost periodic structures," *SBMOI/IEEE MTT-S International Microwave and Optoelectronics Conference*, 427–431, 2009.
5. El Gouzi, M. E. A. and M. Boussouis, "Hybrid method for analyse discontinuities in shielded microstrip," *International Journal of Engineering Science and Technology*, Vol. 2, No. 7, 2010.
6. Eleftheriades, G. V. and J. R. Mosig, "On the network characterization of planar passive circuits using the method of moments," *IEEE Transaction on Microwave Theory and Techniques*, Vol. 44, No. 3, 438–445, Mar. 1996.
7. Bhattacharyya, K. A., *Phased Array Antennas: Floquet Analysis, Synthesis, BFNs, and Active Array Systems*, Wiley and Sons, Mar. 2006.

8. Chou, H.-T., L.-R. Kuo, and S.-C. Tuan, "General analysis of Floquet modes for an one-dimensional,infinite phased array antennas," *IEEE Antennas and Propagation Society International Symposium (APSURSI)*, 1–2, Chicago, IL, Jul. 2012.
9. Valerio, G., P. Baccarelli, P. Burghignoli, A. Galli, R. Rodrguez-Berral, and F. Mesa, "Analysis of periodic shielded microstrip lines excited by nonperiodic sources through the array scanning method," *Radio Science*, Vol. 43, 2008.
10. Bhattacharyya, K. A., "Floquet modal based analysis of finite and infinite phased array antennas," *Macquarie University and IEEE Joint Lecture*, Vol. 43, No. 1, Nov. 2012.
11. Watanabe, K. and K. Yasumoto, "Two-dimensional electromagnetic scattering of non-plane incident waves by periodic structures," *Progress In Electromagnetics Research*, Vol. 74, 241–271, 2007.
12. Mili, S., C. Larbi Aguili, and T. Aguili, "Study of fractal-shaped structures with pin diodes using the multi-scale method combined to the generalized equivalent circuit modeling," *Progress In Electromagnetics Research B*, Vol. 27, 213–233, 2011.
13. Rodrguez-Berral, R., F. Mesa, P. Baccarelli, and P. Burghignoli, "Excitation of a periodic microstrip line by an aperiodic delta-gap source," *IEEE Trans. Antennas Propagat. Letters*, Vol. 8, 641–644, 2009.
14. Watanabe, K., "Spectral-domain approach to electromagnetic scattering from imperfectly periodic," *13th International Conference on Mathematical Methods in Electromagnetic Theory*, 1–6, Ukraine, Sep. 2010.
15. Sze, K. Y. and L. Shafai, "Reflection properties of infinite periodic arrays of rectangular conducting patches," *Can. J. Elect. Comput. Eng.*, Vol. 24, No. 1, Jan. 1999.
16. Skrivervik, K. and L. R. Mosig, "Finite phased array of microstrip patch antennas: The infinite array approach," *IEEE Trans. Antennas Propagat.*, Vol. 40, No. 5, 579–582, 1992.
17. Craeye, C., "Expoitation of infinte-array results for accurate solution of finite widebands arrays," *EMTS*, 2007.
18. Baudrand, H., *Circuits Passifs en Hyperfréquences*, Editions Cépaduès, Jan. 2001.
19. BenSalah, T., C. L. Aguili, and T. Aguili, "Renormalization group application to multi-port model for studying fractal-shaped structures' diffraction," *PIERS Proceedings*, 1629–1633, Beijing, China, Mar. 23–27, 2009.
20. Ayari, M., T. Aguili, H. Temimi, and H. Baudrand, "An extended version of transverse wave approach (TWA) for full-wave investigation of planar structures," *Journal of Microwaves, Optoelectronics and Electromagnetic Applications*, Vol. 7, No. 2, Dec. 2008.
21. Makarov, S., A. Puzella, and V. Iyer, "Scan impedance for an infinite dipole array: Accurate theoretical model compared to numerical software," *IEEE Antennas and Propagation Magazine*, Vol. 50, 132–149, Dec. 2008.
22. Zhang, K. and D. Li, *Electromagnetic Theory for Microwaves and Optoelectronics*, Springer, Berlin, Heidelberg, New York, 1998.
23. Vardaxoglou, J. C., *Frequency Selective Surfaces, Analysis and Design*, John Wiley and Sons, 1997.
24. Mekkioui, Z. and H. Baudrand, "A full-wave analysis of uniform microstrip leaky-wave antenna with arbitrary metallic strips," *Electromagnetics*, Vol. 28, No. 4, 296–314, 2008.
25. Riabi, M. L., M. Ahmadpanah, H. Benzina, H. Baudrand, and V. Fouad Hanna, "Performance of the LSBRM using efficient weighting functions for planar structures," *IEEE Trans. Antennas Propagat.*, Vol. 142, No. 4, 364–368, Aug. 1995.
26. Aguili, T., "Modélisation des composants S. H. F planaires par la méthode des circuits équivalents généralisés," Thesis, National Engineering School of Tunis ENIT, May 2000.
27. Sultan, K. S., H. H. Abdullah, and E. A. Abdallah, "Method of moments analysis for antenna arrays with optimum memory and time consumption," *PIERS Proceedings*, 1353–1356, Kuala Lumpur, Malaysia, Mar. 27–30, 2012.
28. Li, D. and C. D. Sarris, "Efficient finite-difference time-domain modeling of periodic structures under non-periodic sources," *Antennas and Propagation Society International Symposium*, 2007.